2.5 MRMS QPE PERFORMANCE DURING THE 2013-14 COOL SEASON

Stephen B. Cocks* and Steven M. Martinaitis
OU/CIMMS and NOAA/OAR/NSSL, Norman, Oklahoma

Jian Zhang and Kenneth Howard
NOAA/OAR/NSSL, Norman, Oklahoma

1. INTRODUCTION

Multi-Radar Multi-Sensor (MRMS) Quantitative Precipitation Estimate (QPE) products have been transitioned into the National Weather Service (NWS) operations at the National Center for Environmental Predictions (NCEP) (Zhang et al., 2014). As part of this transition, a systematic validation and verification effort is under-way to characterize the MRMS performance in meteorological, aviation and hydrological applications. This study examined the MRMS QPE performance for weather events occurring from December 2013 through March 2014 with a variety of areal coverage and precipitation types. While this study is limited to weather events that occurred east of the Rocky Mountains, a companion study is in progress that encompasses the inter-mountain regions (Martinaitis et al. 2014). Evaluations of QPE almost always involve an inter-comparison of radar rainfall estimates to rain gauge accumulations. There are a number of limitations that must be considered during these types of detailed evaluations. Ground clutter, blockage and non-meteorological echoes can contaminate the lower elevation angles; however, the extra information provided by Dual-Polarization (DP) data has been used by MRMS to mitigate these effects (Tang et al. 2014). Increased sampling volume at greater distances (Steiner et al. 1999), beam overshoot and bright banding in the melting layer (Smith et al. 1996), improper calibration, and use of improper reflectivity-to-rain (Z-R) relationships (Wilson and Brandes 1974; Steiner et. al 1999) can significantly affect radar derived rainfall estimates. Conversely, blockages and poor site placement (Sieck et. al 2007; Fiebrich et al. 2010), gauge undercatch due to strong winds (Wilson and Brandes 1974; Sieck et. al 2007), power outages preventing data transmission (Martinaitis 2008), mechanical malfunctions, telemetry and transmission problems (Groisman and Legates 1994; Marzen and Fuelber 2005; Kim et al. 2009) can contribute to gauge errors. As the study progressed, it was readily apparent that some of these error factors were present in this study. In particular, analysis indicated a number of the automated reporting gauges during winter weather events were becoming clogged, or "stuck," due to frozen precipitation (Martinaitis et al. 2014). This adversely affected precipitation products that used hourly automated gauges to adjust radar estimates. Therefore, this paper documented the performance of the MRMS QPE radar-only (Q3RAD, Zhang et al. 2014), the mosaic Dual Pol. (DPR, Giangrande and Ryzhkov, 2008) and the NCEP Stage II (SII, Lin and Mitchell, 2005) products for eleven precipitation events during the 2013-2014 cool season over the United States east of the Rockies.

2. DATA METHODOLOGY AND QUALITY CONTROL MEASURES

Eleven weather events between December 2013 and March 2014 were chosen for the evaluation (see Appendix). The events evaluated either had significant areas of rain, where totals were ≥ 51 mm (2.00 in.), significant areas of moderate to heavy snow, or a combination of the two. Upper air, numerical model and radar data combined with radar rainfall and gauge totals were evaluated for 24-hr periods ending at 1200 UTC. Hourly and 24-hr radar derived estimates and gauge accumulations were compared at corresponding grid-point (henceforth called R/G pairs). Approximately 12,000 rain gauges from a variety of national and regional networks are ingested by the MRMS system, including 24-hr precipitation data from the Community Collaborative Rain, Hail & Snow (CoCoRaHS) network and hourly data from Hydro-meteorological Automated Data System (HADS).

---

* *Corresponding author address:* Stephen B. Cocks, National Weather Center, 120 David L. Boren Blvd. Suite 4730, Norman, OK 73072;
E-mail: stephen.cocks@noaa.gov

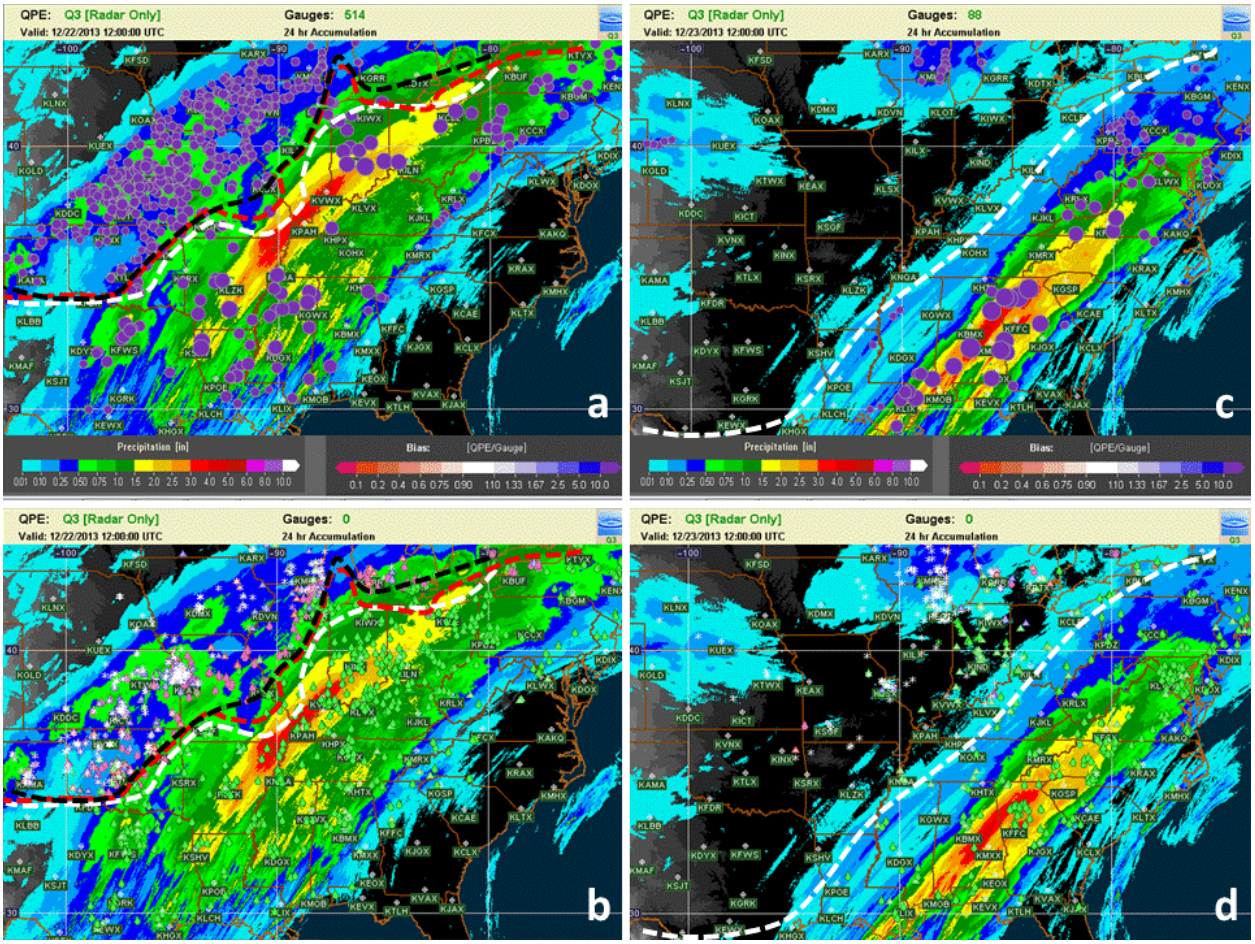

Figure 1. *Q3RAD 24-hr QPE ending at 1200 UTC 22 December 2013 (a, b) and 23 December 2013 (c, d). Locations where gauge totals report ≤ 0.25 mm (0.01 in.) and Q3RAD ≥ 6.4 mm (0.25 in.) denoted by the filled purple bias circles. Dashed lines denotes the RAP model analysis 0°C surface temperature at 1800 UTC 21 December (black), 0000 UTC 22 December (red) and 1200 UTC 22 December (white).*

CoCoRaHS gauge totals are reported by volunteer observers trained to monitor and report both liquid and frozen precipitation types measured by catchment rain gauges. HADS gauges are automated with the primary gauge type being the heated tipping bucket variety. The previously mentioned challenges with gauge performance during frozen precipitation were prevalent in this study. Figure 1 shows the Q3RAD 24-hr precipitation estimate ending at 1200 UTC 22 December 2013 and 23 December 2014. Meteorological Phenomena Identification Near the Ground (mPING) and synoptic reports confirmed model analysis data that frozen precipitation was falling across the region where the large majority of the gauges indicated that none or very little precipitation was measured. There were some gauges in regions with above freezing surface temperatures that were also likely stuck, clogged or malfunctioning. However, these were outnumbered by a factor of four by suspect gauges located in freezing temperatures.

Almost all of these suspect gauges were automated and their presence had a significant impact on performance statistics as well as the MRMS locally gauge corrected radar QPE (Q3GC) product (Zhang et al. 2011, 2014). Figure 2 shows the Q3RAD and Q3GC estimates for the same time, with Q3GC adjusted based on hourly automatic gauge data. National Weather Service analysis (not shown) confirmed that a swath of moderate to heavy snow fell in this region with snowfall totals from 100 mm (4.00 in.) to 200 mm (8.00 in.) with locally higher amounts. The presence of hundreds of stuck gauges removed the precipitation maximum behind the freezing line in the Q3GC product. This example was not an isolated event as large numbers of suspect gauges during other precipitation events adversely affected the Q3GC product. Therefore, the

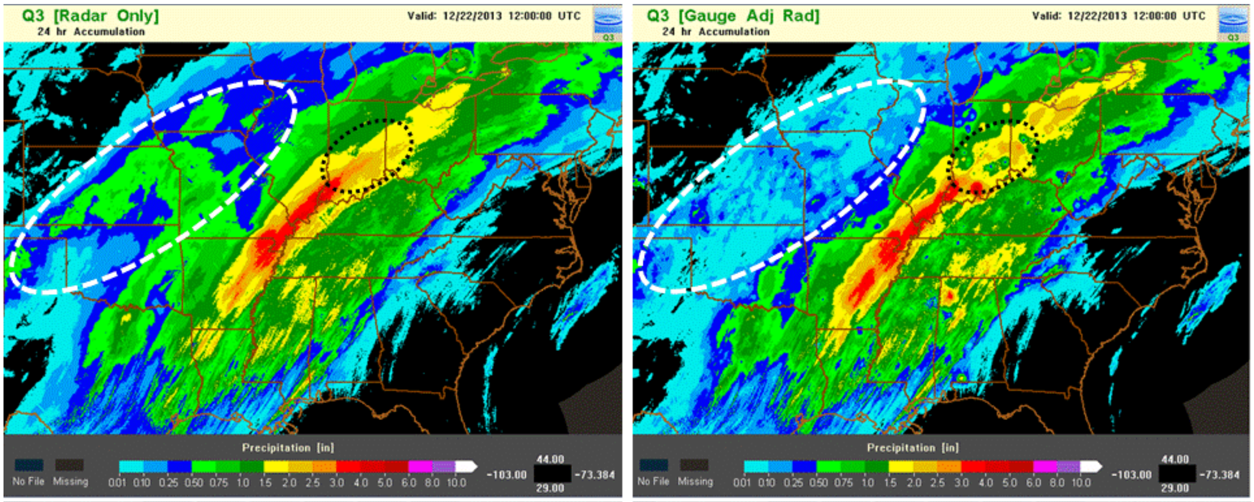

Figure 2. *Q3RAD (left) and Q3GC (right) 24-hr QPE ending at 1200 UTC 22 December 2013. White dashed ovals indicate major differences between the two products. Black dotted ovals indicate effects caused by stuck gauges.*

authors did not evaluate the Q3GC product or any other gauge adjusted product. Instead, the following products were evaluated: Q3RAD, Mosaic Dual Pol. (DPR) and the NCEP Stage II radar-based (hereafter, SII) precipitation estimates. The process for creating DPR mosaics is to first sum hourly Dual Pol. accumulations from the Level III data from the Weather Surveillance Radar-1988 Doppler (WSR-88D) Next Generation Radar (NEXRAD) network. MRMS uses a 'nearest neighbor' approach to determine which Dual Pol estimates to assign to a grid-point; essentially, the estimates from the radar closest to the coordinate was used. There is no attempt to smooth the discontinuities that resulted from such a mosaic as the boundaries between the radars highlighted any radar-to-radar precipitation estimate inconsistencies that may be related to reflectivity, differential reflectivity or hydro-meteorological classification algorithm (HCA) differences. The SII products are developed from WSR-88D NEXRAD data transmitted to NCEP in real-time. Individual WSR-88D radar rainfall estimates are merged onto a national 4 km resolution grid. Inputs from multiple radars are averaged using an inverse distance weighting formula (see Q&A, Stage II at http://www.emc.ncep.noaa.gov/mmb/ylin/pcpanl/QandA/ for details). The performance of these three radar-only products was compared to the NCEP Stage IV (SIV) product which uses a combination of quality controlled WSR-88D, satellite and rain gauge data to create a refined rainfall estimate analysis. While the SIV product is not a real-time product for most operational forecasters, it has

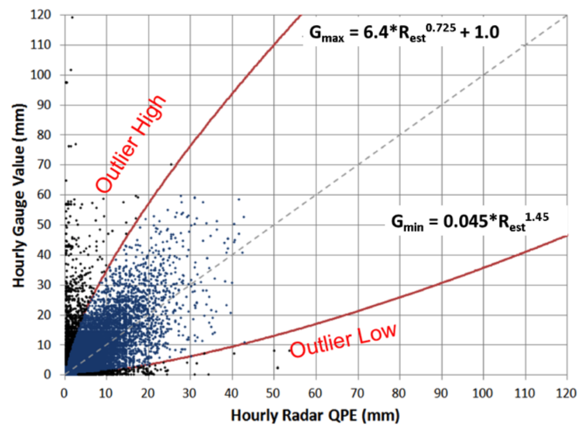

Figure 3 *Power laws used to assist in quality control of R/G pairs. The upper (lower) curve represents the upper (lower) bound for gauge values for a given Q3 hourly total.*

served as the standard for rainfall estimates within the hydrological community.

Because of the problem with gauges becoming stuck in below freezing temperatures, we chose to assess performance based on comparisons between the aforementioned radar only products and 24-hr accumulations from CoCoRaHS gauges. CoCoRaHS gauges have been found to be more consistent and suitable in previous performance assessments. As a minimal quality control measure to reduce erroneous totals, both Q3RAD and the CoCoRaHS gauges were required to be ≥ 2.5 mm (0.10 in.) before including the pair into the analysis. Performance assessment statistics were generated based on all

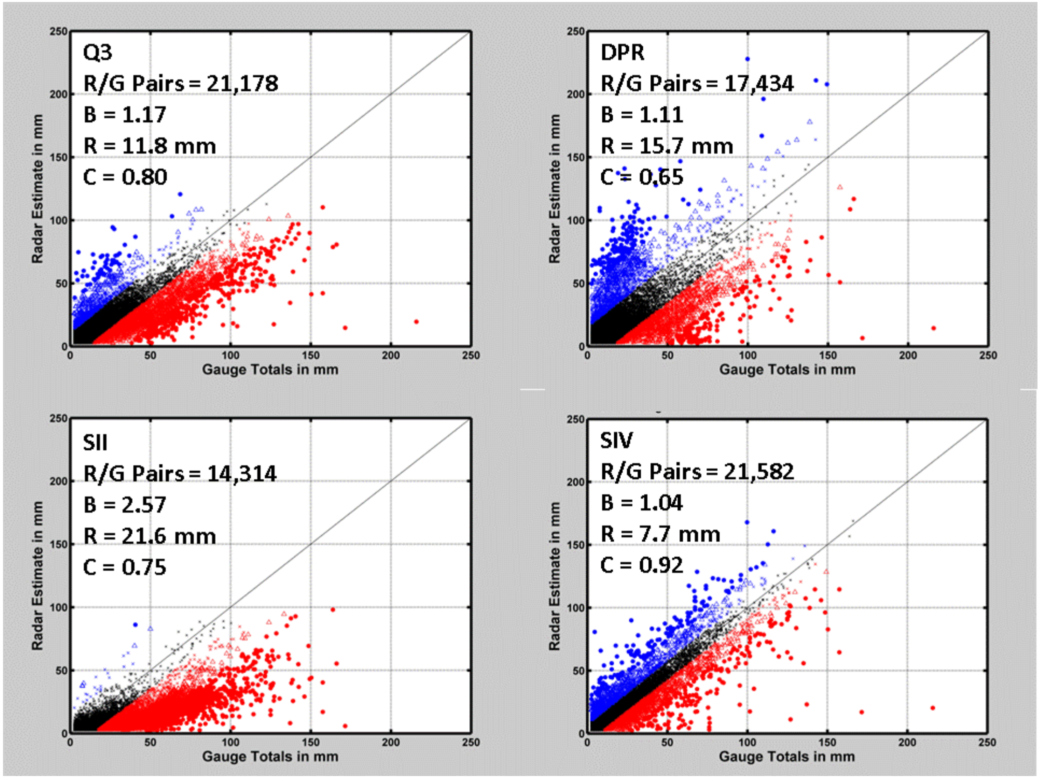

Figure 4. *24-hr QPE from Q3RAD (top left), DPR (top right), SII (bottom left), and SIV (bottom right) vs. CoCoRaHS gauges for all cool season cases. Blue (red) denote over (under)-estimates. Black denotes R/G pairs within one standard deviation. Colored x's, circled x's and dots represent pairs greater than the 1st, 2nd and 3rd standard deviation. 'G' denotes number of gauges, 'B' bias, 'R' RMSE and 'C' correlation coefficient.*

available R/G pairs and by pairs stratified by 24 hour gauge totals ≤ 6.4 mm (0.25 in), ≤ 12.7 mm (0.50 in), > 25.4 mm (1.0 in) and > 50.8 mm (2.0 in). For statistical measures we used a mean bias ratio, defined as the ratio of the gauge total to radar estimate, Root Mean Square Error (RMSE), and correlation coefficient to evaluate the product performance. For time series analysis and diagnosing error trends, HADS hourly data were used with rigorous quality control (QC) measures. QC was primarily applied via a set of thresholds used to determine whether the gauge total, when compared to the radar estimate, was reasonable. Two power laws, that describe an upper and lower gauge total threshold, were developed from gauge/Q3RAD estimates collected during August 2013 (Fig. 3). If a gauge report did not meet these threshold values, the report was considered suspect. While this technique is not perfect, it was effective in identifying and removing gauges that were likely suspect.

3. STATISTICAL ANALYSIS AND RESULTS

Figure 4 and Table 1 show the scatter plot and the cool season statistical results for 24-hr accumulations. The extensively quality controlled SIV estimates had the best overall performance with the lowest RMSE, highest correlation coefficient and the least bias for all accumulation stratifications. Q3RAD estimates had the second best performance as indicated by the RMSE and correlation coefficient statistics. However, the scatter plot and table 1 indicate Q3RAD tends to underestimate totals during the higher precipitation events. While DPR had some statistics better than the SII estimates, it has more variability as easily seen in the scatter plots. The increased variability was likely related to differential reflectivity (ZDR) calibration errors within the NEXRAD network and melting layer precipitation estimate challenges. The former will continue to improve as new procedures are developed to reduce ZDR calibration errors (Cunningham et al. 2013; Hoban et al. 2014) while additional techniques, such as vertical profile of reflectivity (VPR) corrections of bright band contamination, are being considered for the latter. Overall, the SII estimates had the overall lowest statistics with a

Table 1. *Bias, RMSE and correlation for each precipitation estimation product stratified by gauge amount.*

Product	***24 hr Gauge Amount***	***# R/G Pairs***	***Bias***	***RMSE (mm)***	***Correlation***
Q3RAD	*G ≤ 6.4 mm (0.25 in.)*	3,975	0.59	5.9	0.11
	G ≤ 12.7 mm (0.50 in.)	9,524	0.80	6.1	0.27
	G > 12.7 mm (0.50 in.)	11,654	1.29	14.9	0.74
	G > 25.4 mm (1.00 in.)	5,452	1.40	19.9	0.68
	G > 50.8 mm (2.00 in.)	1,589	1.51	29.5	0.56
DPR	*G ≤ 6.4 mm (0.25 in.)*	2,958	0.55	8.0	0.08
	G ≤ 12.7 mm (0.50 in.)	7,411	0.76	8.9	0.20
	G > 12.7 mm (0.50 in.)	9,988	1.21	19.3	0.58
	G > 25.4 mm (1.00 in.)	4,790	1.34	23.7	0.54
	G > 50.8 mm (2.00 in.)	1,416	1.44	31.8	0.56
SII	*G ≤ 6.4 mm (0.25 in.)*	1,052	1.01	2.9	0.02
	G ≤ 12.7 mm (0.50 in.)	3,871	1.69	5.2	0.09
	G > 12.7 mm (0.50 in.)	10,443	2.71	25.1	0.73
	G > 25.4 mm (1.00 in.)	5,335	2.73	32.8	0.67
	G > 50.8 mm (2.00 in.)	1,582	2.60	47.1	0.53
SIV	*G ≤ 6.4 mm (0.25 in.)*	4,268	0.71	4.2	0.16
	G ≤ 12.7 mm (0.50 in.)	9,883	0.88	4.4	0.43
	G > 12.7 mm (0.50 in.)	11,699	1.08	9.6	0.89
	G > 25.4 mm (1.00 in.)	5,459	1.08	12.5	0.84
	G > 50.8 mm (2.00 in.)	1,590	1.08	17.7	0.66

strong tendency to underestimate precipitation; however its consistency makes it more easily correctable, via a bias adjustment or gauge correction, than DPR estimates.

Table 1 confirms that all of the radar only estimates tended to underestimate in moderate to heavy precipitation to varying degrees. The bias and RMSE increased while correlation coefficient decreased for the higher precipitation total stratifications. This is not surprising as radar beam overshoot is more common during the cool season due to shallower precipitation systems and lower cloud bases; however, the degree which the SII product underestimates precipitation totals when compared to the Q3RAD and DPR was surprising. Radar beam overshoot should be partly mitigated in all of the products due to the various radar mosaic processes used. We speculate that the real difference in terms of the magnitude of the under-estimates between SII and Q3RAD/DPR is the latter two uses radar echo classifications to determine the Z-R relationship used to calculate precipitation. SII uses the same Z-R relationship for the entire radar field and is chosen by the forecaster with regards to the synoptic or meso-scale situation. All of the products tend to have lower correlation and a distinct overestimate bias for lighter precipitation totals (i.e., ≤ 12.7 mm). A significant portion of these errors are likely due to precipitation evaporating/ sublimating before reaching the ground, gauges impacted by frozen precipitation but passed the QC threshold or a combination of both. An advancement of the VPR algorithm was installed this past spring to help mitigate these types of errors in MRMS by comparing multiple radar observations at an overlapping point and ensuring the lowest radar bin has significant echoes present before coding a geographical point as having precipitation. However, it will still be unable to determine whether echoes seen at the lowest radar bin actually reaches the ground, especially at farther ranges.

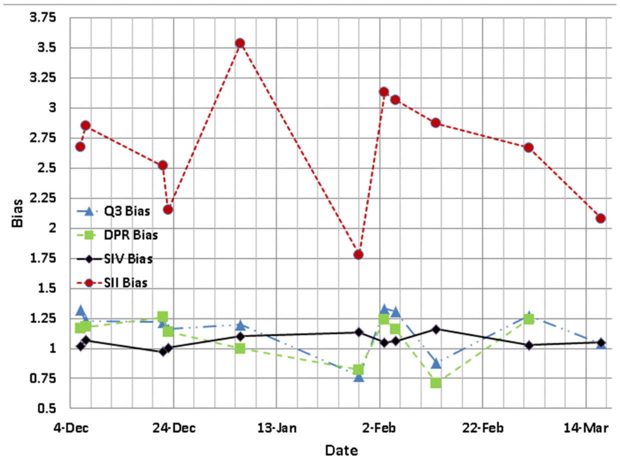

Figure 5. *Q3RAD (blue dashed line, triangles), DPR (green dashed line, squares), SII (red dashed line, circles) and SIV (black solid line, diamonds) mean bias ratio statistics for each cool season case evaluated.*

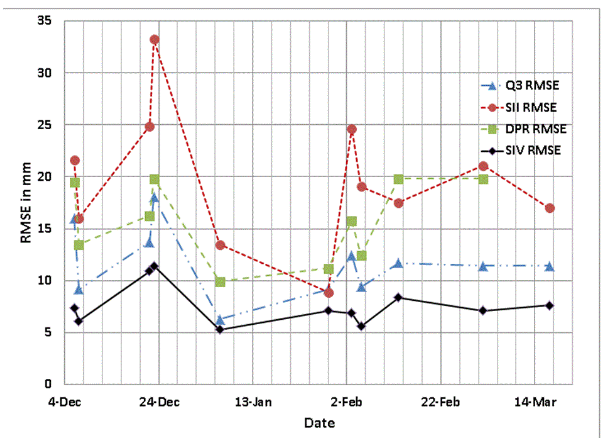

Figure 6. *Same as Figure 5 except for RMSE.*

4. EVENT-BY-EVENT RESULTS AND NOTABLE EXAMPLES

Figure 5 shows the mean bias ratio for each precipitation estimate product during each cool season event. The bias for SII was generally above 2.00 for all evaluated events. We view the SII radar only product as a mosaic proxy for the Precipitation Processing System (PPS), while Q3RAD, DPR, and SIV represent more recent precipitation estimate developments. The large differences between SII and the other precipitation estimates, in a way, reflect the progress that has been made over the past fifteen years to further improve precipitation estimates and hence improve operational hydrological forecasting. The bias for the SIV product is closer to one than Q3RAD and DPR because of the inclusion of quality controlled gauge observations by forecasters. However, the Q3RAD bias showed encouraging results for an automated real-time product; DPR is also fairly close to 'one' but as mentioned previously there is also a lot of scatter associated with the estimates. The overall best correlation values (not shown) were consistently found with the SIV product followed next by Q3RAD, DPR and SII. The SII product had the higher RMSE errors in most cases with SIV having the lowest RMSE (fig. 6). Q3RAD was comparable, within 5.0 mm (0.20 in.), to SIV in the majority of the cases. The DPR RMSE errors (correlation) were likely higher (lower) due to the calibration and melting layer challenges mentioned previously. The following are some notable examples where DPR had difficulties estimating rain within the melting layer.

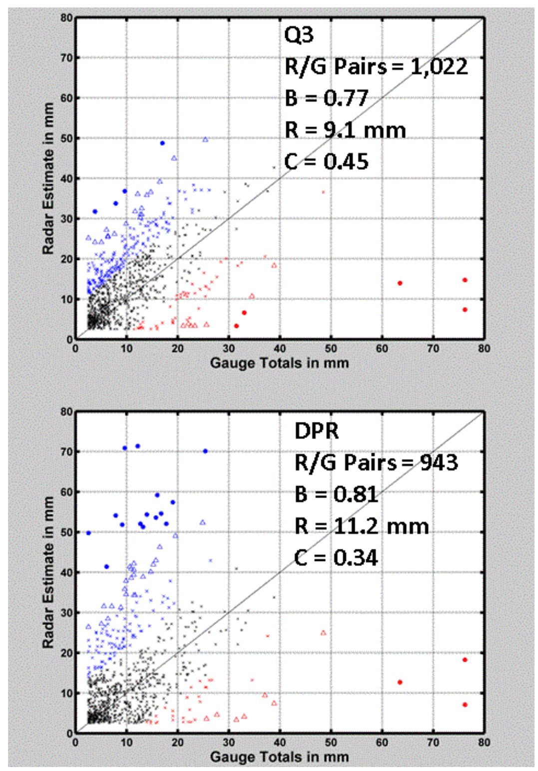

Figure 7*: Q3RAD (top) and DPR (bottom) estimates vs CoCoRaHS gauge totals for the 24-hr period ending 12:00 UTC, 29 January 2014 with legend same as figure 4.*

4.1. SOUTHEASTERN U.S. PRECIPITATION EVENT OF 28-29 JANUARY, 2014

An arctic air mass was in place over much of the southeastern U.S. on the 28th and 29th of January, 2014. An upper trough, jet stream

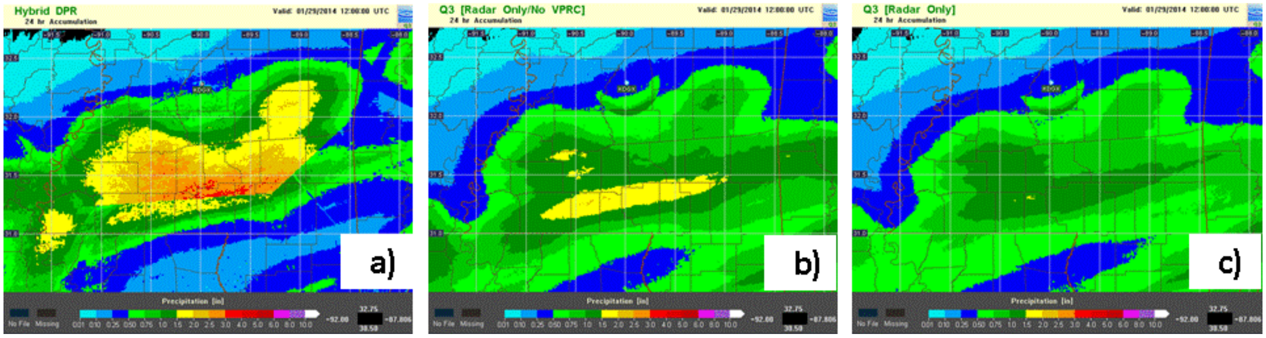

***Figure 8**: DPR (a), Q3RAD not corrected for bright band contamination (b) and Q3RAD (c) estimates for the 24-hr period ending 12:00 UTC, 29 January 2014.*

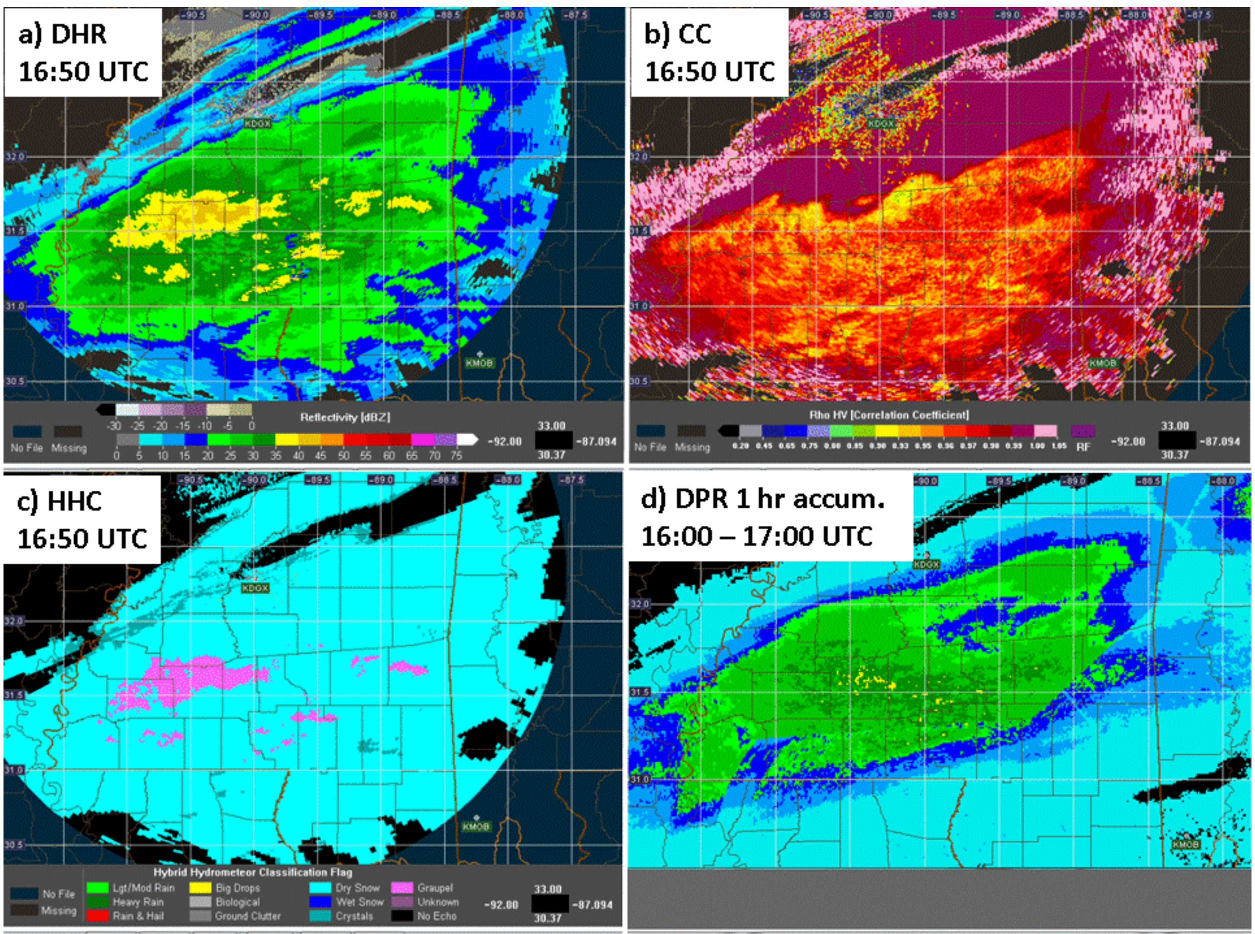

***Figure 9**: Digital hybrid scan reflectivity (a), correlation coefficient (b) and hybrid-hydro meteorological classification algorithm (c) images from the Jackson, Mississippi WSR-88D at 16:50 UTC, 28 January 2014. Dual Pol. precipitation estimate (d) for the 1-hr period ending 17:00 UTC of the same date.*

dynamics and moisture flowing over the colder air resulted in the development of freezing rain, sleet and snow over large sections of the region. Fig. 7 shows the scatter plots for the radar only products. Both Q3RAD and DPR had a significant amount of scatter and there was a distinct over-estimate bias present in this event. The DPR plot is notable as it has an even stronger over-estimate signature than Q3RAD. Calibration of radar reflectivity (Z) and differential reflectivity (ZDR) was evaluated using the Radar Reflectivity Comparison Tool (RRCT, available at: http://rrct.nwc.ou.edu/). Most radar Z values appeared to be within +/– 1 dBZ of each other. It is harder to discern ZDR calibration across the network as it is difficult to measure the ZDR bias with high precision. A ZDR bias higher than 0.25 dBZ can substantially reduce the performance of Z/ZDR based rain estimates. Overall, there were some radars that clearly had biases above 0.30 dBZ while others it was harder to determine as the value lay between 0.15 and 0.30 dBZ. Suffice to say that ZDR calibration likely affected some of the precipitation estimates; however much of the area was below freezing at the surface and as a result precipitation estimates calculating rain rates using Z and ZDR (R(Z,ZDR)) were infrequent for this case.

Besides calibration induced errors, melting layer overestimates were noted in the DPR estimate data. Fig 8 shows the 24 hour totals around the Jackson, Mississippi WSR-88D radar (KDGX). The DPR estimates exhibited maximum liquid precipitation totals of 50 to 76 mm (2.0 – 3.0 in), substantially more than the Q3RAD or even the Q3RAD estimate uncorrected for bright band contamination. The Q3RAD estimate without bright band correction applied was lower than the DPR estimate for two reasons. The first is related to the MRMS mosaic process used to develop the reflectivity field. If more than one radar is available for a grid-point a weighted mean is taken (Zhang et al., 2011) which may act to smooth out spuriously high reflectivities. Second, once the mosaic reflectivity field is created a unique Z-R relationship is applied, either a cool ($Z = 75*R^2$ where 'R' represents rain rate) or a warm ($Z = 200*R^{1.6}$) season equation. This is in contrast to what is used by the DPR estimates which uses the convective Z-R relationship ($Z = 300*R^{1.4}$), multiplied by a coefficient, for hybrid hydro-meteorological classification algorithm (HHC) classifications in and above the melting layer and for any graupel or wet snow classifications below the melting layer. Fig. 9 showed the digital hybrid reflectivity (DHR), correlation coefficient (CC), hybrid hydro-meteorological classification algorithm (HHC) and the one-hour DPR estimate for the Jackson, Mississippi WSR-88D (KDGX) during a period where the highest one-hour DPR accumulations were generated. A calibration check of the KDGX radar indicated it appeared reasonably calibrated in Z although it showed a significantly high bias (at least 0.4 dBZ) in ZDR. The CC data clearly indicated a melting layer to the south of the radar but precipitation had re-frozen by the time it reached the ground as indicated by surface observations (not shown). The HHC between 16:00 and 17:00 UTC classified radar echoes as either dry snow, the most common classification, or as graupel (in areas with higher reflectivity). For these classifications, the Dual Pol. Quantitative Precipitation Estimate (DP QPE) algorithm estimated precipitation via the convective Z-R relationship multiplied by a coefficient (as determined by the HHC class). Regardless, the DPR totals are quite high throughout the melting layer which is due not only to bright band contamination but likely the use of the convective Z-R relationship.

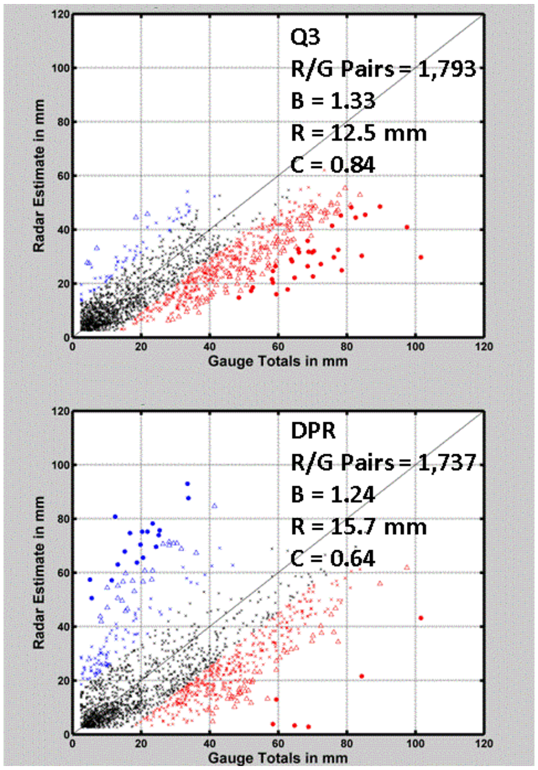

***Figure 10**: Q3RAD (top) and DPR (bottom) estimates vs CoCoRaHS gauge totals for the 24-hr period ending 12:00 UTC, 03 February 2014 with legend same as figure 4.*

Ground truth from hourly automatic gauges in the bright-band affected region around KDGX was practically non-existent as most were substantially impacted by a combination of freezing rain, sleet, or snow. However, there were five CoCoRaHs gauges within the bright band region that were available for comparison. The absolute value of the DPR minus gauge 24-hr accumulation error within the melting layer region averaged 37.2 mm (1.47 in); in contrast, the magnitude of the Q3RAD minus gauge error was 14.2 mm (0.56 in) representing about a 62% reduction in the error. While it is true that the CoCoRaHs gauges may have suffered some impacts such as gauge under-

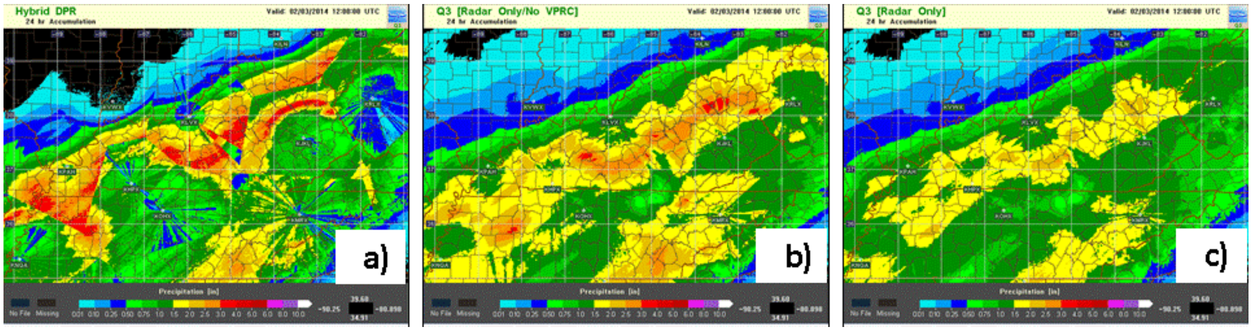

***Figure 11**: DPR (a), Q3RAD not corrected for bright band contamination (b) and Q3RAD (c) estimates for the 24-hr period ending 12:00 UTC, 03 February 2014.*

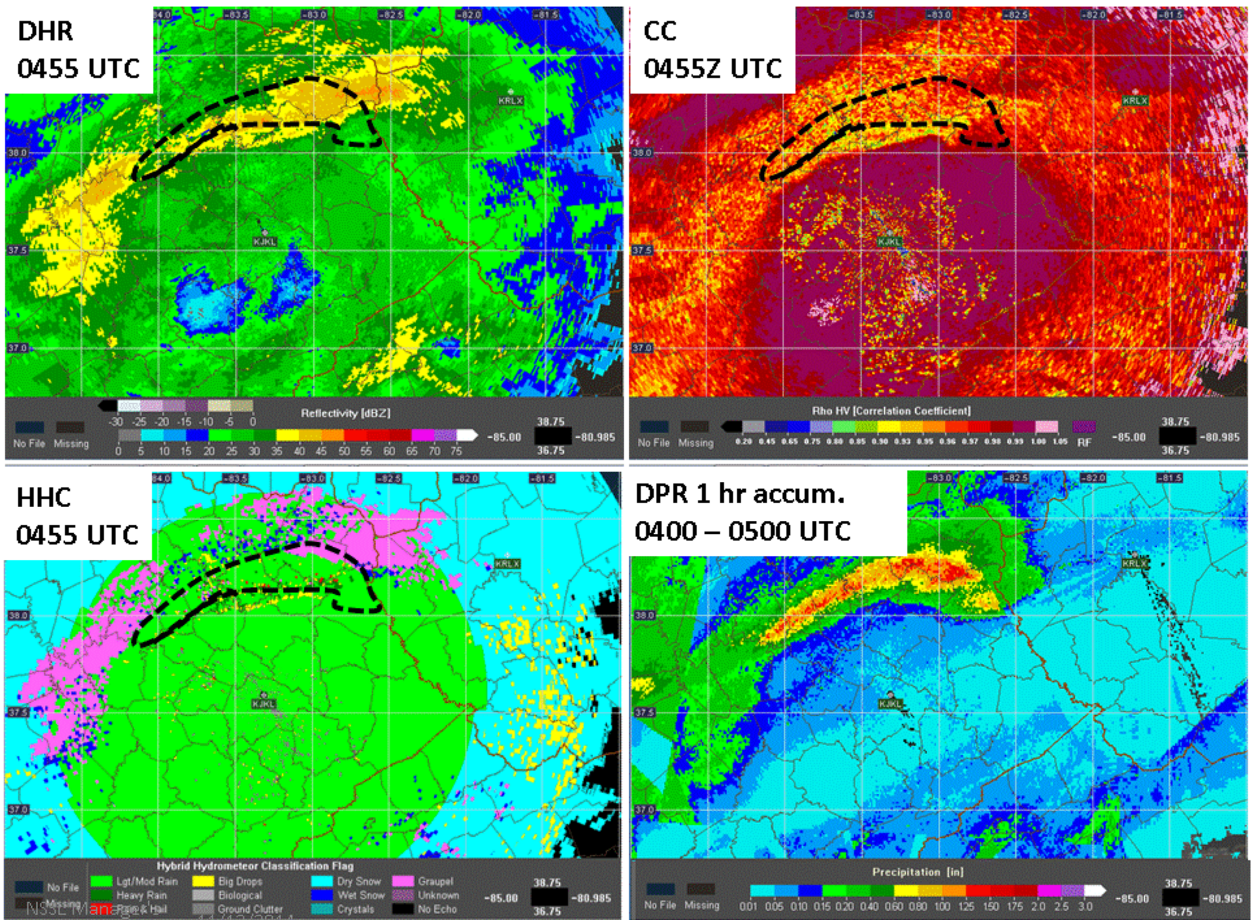

***Figure 12**: DHR (a), CC (b) and HHC (c) images from the Jackson, Kentucky WSR-88D at 04:55 UTC, 03 February 2014. Dual Pol. precipitation estimate (d) for the 1-hr period ending 05:00 UTC of the same date. Dashed black line represents highest 1-hr DPR accumulations.*

catch in snow and/or ice accumulation within the catchment, volunteers are trained in handling these situations so these amounts are the best estimates to what actually reached the ground in the area of interest.

4.2. OHIO VALLEY/SOUTHEASTERN U.S. PRECIPITATION EVENT OF 02-03 FEBRUARY, 2014

A cold front, associated with arctic air, was slowly moving eastward across the Ohio Valley and the Southeast U.S on the 02nd and 03rd of February, 2014. Frozen precipitation was in progress over portions of Indiana and northwest Ohio while rain was occurring southward as moisture was isentropically lifted up and over the colder air. Another area of precipitation, further southwest of the Ohio Valley region, developed in advance of a 500 hPa short wave. This area of precipitation moved east-northeastward into the region by the evening of the 2^{nd} resulting in moderate to heavy rainfall in the Southeast and a variety of precipitation types over portions of the Ohio Valley and the Appalachian Mountains. Fig 10 shows the Q3RAD and DPR scatter plots for this event; the DPR plot is very similar to that seen in the previous case. A check of radar calibration across the area indicated the Paducah, Kentucky (KPAH), Wilmington, Ohio (KILN), Evansville, Indiana (KVWX) and the Knoxville, Tennessee (KMRX) WSR-88Ds were at least 1.0 dBZ too warm or too cool respectively. Otherwise, the rest of the radars in the region were within +/– 1 dBZ. With a couple of exceptions, most radar ZDR values were within 0.15 to 0.30 dBZ of each other. As previously noted, a ZDR bias above 0.25 dBZ will affect R(Z,ZDR). Therefore, it is likely Z and ZDR calibration errors affected some of the radar estimates.

Fig 11 showed the 24-hr accumulations for DPR, Q3RAD uncorrected and Q3RAD. Both, the DPR and Q3RAD uncorrected estimates exhibited 'hot' spots of high accumulation in the same general vicinity; some in the shape of distinct arcs. The DPR QPE around the Jackson, Kentucky WSR-88D (KJKL) formed a nearly 180^0 arc. The Q3RAD, which was corrected for bright band contamination, showed much lower totals across the region. Fig. 12 shows DHR, CC, HHC data and the one-hour DPR estimate for the KJKL radar during a time where the highest one-hour DPR accumulations were being generated. This radar was reasonably calibrated in Z and the ZDR bias was between 0.15 and 0.30 dBZ. At the surface, frozen precipitation was occurring over the northwest half of the radars field of view while rain was occurring elsewhere. The CC data between 04:00 and 05:00Z clearly indicated a melting layer coinciding with higher reflectivity; over the region of higher DPR accumulations the HHC classified echoes primarily as light/moderate rain. For this HHC class, the rain rate is derived using an expression, dependent upon Z and ZDR, originally derived for warm season precipitation with tropical characteristics. A comparison of DPR estimates with seven available CoCoRaHs gauges within the region of greatest DPR 24 hour accumulations (the arc region) was made to estimate the average error. In contrast to the previous case, there were a number of hours when liquid precipitation occurred within the area of interest before transitioning to frozen precipitation. The absolute value of the DPR minus gauge error within the area of interest averaged 33.8 mm (1.33 in); in contrast, the magnitude of the Q3RAD minus gauge error was 11.5 mm (0.46 in), a nearly two thirds reduction. It should be noted that there were a couple of gauge sites where Q3RAD actually under-estimated when compared to the CoCoRaHs 24-hr totals, indicating the VPR correction may have been too aggressive. However, the error magnitudes observed were substantially lower than that seen with DPR for each gauge.

5. Q3RAD PRECIPITATION TYPE ANALYSIS

Analysis was conducted of the MRMS precipitation type contributions to the Q3RAD totals for over and under-estimate R/G pairs to better understand what may be causing some of the Q3RAD error trends seen in the statistics. MRMS uses a 'Surface Precipitation Type' algorithm to classify radar data based upon a combination of echo characteristics and model data in order to assign a unique reflectivity-to-rain-rate (Z-R) relationship for each class (Zhang et al. 2011, 2014). There are seven possible precipitation classifications: 1) warm stratiform (WS), 2) cool stratiform (CS), 3) tropical stratiform (TS), 4) convective (CO), 5) hail (HL), 6) tropical convective (TC), and 7) snow (SN). If no radar echoes are present for a given time step, then the pixel in question is assigned the designation 'no echo' (NE). To determine the importance of the stratiform and convective precipitation types to R/G pair over- and under-estimate values, the various classifications were combined into three categories: Stratiform (WS, CS, TS), convective (CO, HL, TC) and snow (SN). While most of the SN classifications were probably stratiform-like radar echoes with model temperatures indicating the surface was at or below freezing, SN was still separated out to identify trends related to challenges with measuring frozen precipitation. To determine what classification categories contributed most to the hourly Q3RAD precipitation estimates the total amount of Q3RAD estimated per time step was calculated for each hourly R/G pair. From this, the total Q3RAD estimate per precipitation classification was summated for all time steps and all hourly R/G pairs. Then the percentage contribution of each

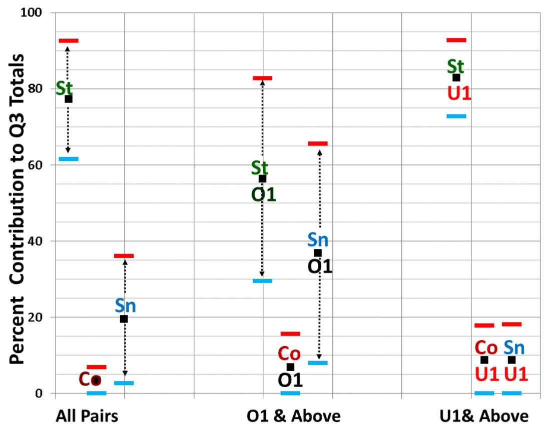

Figure 13. *Percent contribution to Q3RAD totals for all R/G pairs and the first SDE over (O1) and under (U1) estimate R/G pairs. Red and light blue horizontal hashes mark the first SDE uncertainty of the eleven case average. 'St', 'Co' and 'Sn' denote stratiform, convective and snow categories.*

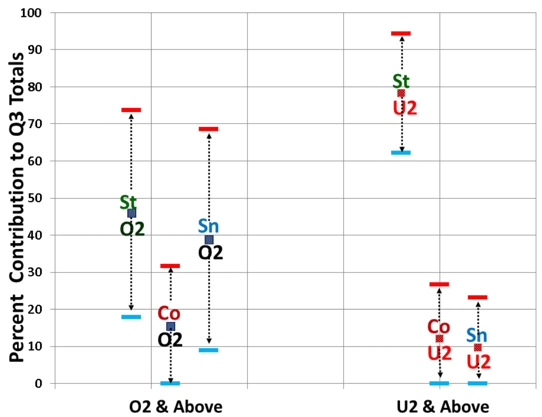

Figure 14. *Same as Figure 8 except for second SDE estimates.*

precipitation classification to the Q3RAD total was calculated. The first and second Standard Deviation Error (SDE) over- and underestimates were determined by examining the hourly radar estimate minus gauge (R – G) errors. There were more than 3.5 times as many 1st SDE underestimates than overestimates in the data, confirming the tendency seen in the Q3RAD vs. CoCoRaHS analysis. The average percent Q3 contribution to the total for each category and the standard deviation of the average for the eleven evaluated cases were calculated and graphed for all R/G pairs and first and second SDE over- and underestimates (Figs. 13, 14).

For all R/G pairs, most of the Q3RAD contribution came from the stratiform rain

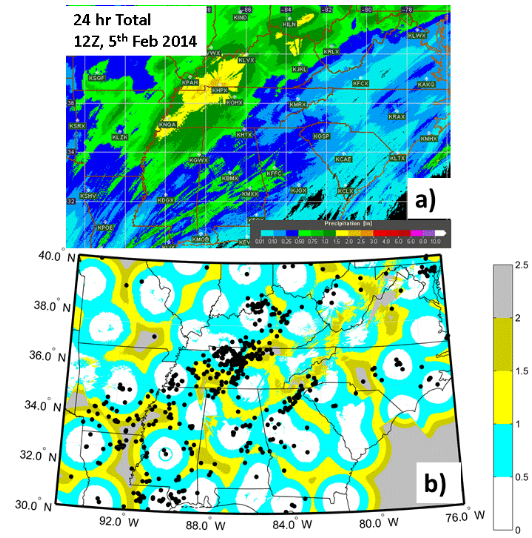

Figure 15. *24-hr Q3RAD accumulation (a) and the height of the bottom of the radar beam (b) with locations of underestimates of at least the first SDE (black dots) for the period ending 1200 UTC 5 February 2014. The height of the bottom of the radar beam is in kilometers.*

categories followed by snow and convection which is not surprising for cool season precipitation events. For 1st SDE overestimate error R/G pairs, most of the contribution came from the stratiform (~56%) and snow (~37%) categories; Convection classifications contributed the least (< 7%) to the Q3RAD totals. Similar results were found for the second SDE overestimate error R/G pairs. The high percentages seen in the snow category likely reflect the difficulty of measuring snowfall, particularly if there is any wind present. A large majority of precipitation gauges experienced a reduction in snowfall catch efficiency that increases with increasing wind speed in a study by Rasmussen et al. (2012). This bias also depends upon the temperature and precipitation characteristics (Goodison and Yang 1996). Another factor that likely played a role in the overestimates associated with the snow classification was poor performance of the automated gauges during frozen precipitation events (Rasmussen et al. 2012; Martinaitis et al. 2014). The high percentages of overestimates in the stratiform category were primarily attributed to the cool stratiform precipitation classification. Examination of some of the cases indicated virga and gauges partially impacted by winter weather were having a significant impact. The virga impact was also noted in the statistical analysis from Table 1 where Q3RAD estimates typically had low correlation and a distinct overestimate bias for 24-

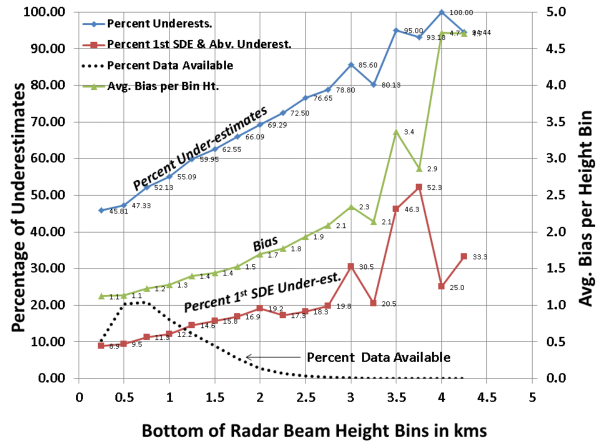

Figure 16. *Percentage of under-estimates (blue), 1st SDE under-estimates (red) and gauge-to-radar estimate bias (green) as a function of radar beam bottom height.*

hr totals ≤ 6.4 mm (0.25 in). Other possible causes for overestimates would be gauge under-catch in light rain, limitations of using Z-R relationships and improper radar calibration.

For 1st SDE underestimate R/G pairs, the chief contribution to the Q3RAD totals were from the stratiform category (82.8%) followed by snow (8.6%) and convection (8.6%). Similar results were found for the 2nd SDE underestimate R/G pairs. Further, the CS classification contributed the most to the under-estimate errors. A significant amount of the error is likely due to the radar beam partially over-shooting the generally lower cloud bases and shallower precipitation systems found during the winter time, an example of which is illustrated in Fig. 15. There were few underestimates from northwestern Arkansas to northwestern Tennessee and north of the Ohio River. This was where temperatures in the previous 24 hours were either near freezing or sub-freezing, and hence, many gauges had likely become stuck or clogged from winter precipitation. In the warmer air, there were a number of under-estimate R/G pairs, a number of which were clustered in regions where the bottom of the radar beam is at least 1 km above ground level. Analyses for the events on 3 February 2014 and 13 February 2014 indicated similar tendencies (not shown). To get a more quantitative look at radar beam over-shoot, the percentage of R – G < 0 (underestimates) was plotted as a function of the seamless hybrid scan reflectivity beam bottom height (H-SHSR) above the ground (see fig. 16). As expected in the winter season, the percentage of underestimates increased linearly from approximately 45% at 0.25 km to near 70% at 2.0 km. However, this effect does not account for under-estimates that resulted from partial beam filling, mis-classification of precipitation types, the limitations of using Z-R relationships and improper radar calibration. Additionally, frozen precipitation and there effects on gauges can even cause an under-estimate bias for radar estimates on some occasions. This can happen when gauges previously stuck or clogged, with ice and snow contained within the gauge orifice, can begin to melt as temperatures rise and new precipitation begins to fall. The thawing frozen precipitation begins to thaw giving the appearance more precipitation is being measured than what actually fell from the clouds (see Martinaitis et al. 2014 for an example).

6. CONCLUSIONS

Examination of eleven weather events east of the Rocky Mountains quickly revealed challenges in evaluating radar precipitation estimates during the cool season. Analysis showed that a large number of automatic gauges were likely becoming stuck in freezing temperatures due to frozen precipitation. Since gauge adjusted radar based QPE relied on these gauges for bias correction, this study evaluated radar-only precipitation estimates to avoid any improper gauge correction impacts. Comparisons with SIV analyses showed that Q3RAD, DPR and SII all had a tendency to underestimate precipitation with SII having a more distinct bias. While DPR had a slightly better bias ratio than Q3RAD, it also had more scatter, which was reflected in the higher RMSE and lower correlation values. The higher DPR scatter is likely related to precipitation estimate challenges within and above the melting layer as noted in a couple of examples. Overall, Q3RAD had bias and correlation statistics that were comparable to SIV data and a RMSE value that averaged 4.1 mm (0.16 in.) higher than SIV. Further examination of the statistics revealed radar only estimates had a distinct underestimation tendency that was more pronounced for higher precipitation amounts. A significant portion of this error could be attributed to radar beam overshoot. The ability of MRMS and the Dual Pol. HCA to utilize multiple Z-R relationships across a radar field may have mitigated the magnitude of Q3RAD and DPR underestimates. For lighter 24-hr precipitation totals, all of the estimate products exhibited a distinct overestimate bias. A significant portion of this error may be related to the presence of precipitation evaporating prior to reaching the ground as well as to gauge undercatch and measurements made from gauges partially impacted by winter precipitation. A review of the statistics of each radar-only estimate per weather event revealed a rather marked difference between SII and the other QPE products, which the authors view as a reflection of the substantial progress made in improving precipitation estimates over the past fifteen years.

An analysis of MRMS precipitation classification contributions to Q3RAD totals indicated the stratiform and snow categories produced the most for overestimate R/G pairs. The chief contributor of the stratiform category to these types of errors was the cool stratiform precipitation type. It is hypothesized that a significant portion of the overestimate errors with the snow and cool stratiform precipitation types were related to gauge performance challenges in freezing temperatures and gauge under-catch in windy conditions. Precipitation evaporating or sublimating prior to reaching the ground likely played a significant role as well. Analysis also indicated that the cool stratiform classification, was associated with underestimate errors with the primary factor being radar beam overshoot although other factors are quite significant as well.

There are several future investigations that are worthy of mentioning as they are related to verification and improvement of precipitation estimates. First, a warm season analysis of precipitation estimates from meso-scale convective systems over the north central Plains and the southeastern U.S. is in progress to assess performance of the radar-only products. Second, work is underway to integrate Dual Pol. information into MRMS Q3RAD precipitation estimates via the use of specific attenuation (Ryzhkov et al., 2014; Wang et al., In Press). Third, a future project will likely examine the feasibility of improving DPR estimates in the melting layer by incorporating a VPR correction of the bright band to WSR-88D products similar to what has been implemented in MRMS (Zhang and Qi, 2010; Zhang et al. 2011). It may also be possible to apply a stratiform Z-R relationship, instead of the convective Z-R, within and above the bright band region to further reduce the error.

7. REFERENCES

Cunningham, J. G., W. D. Zittel, R. R. Lee and R. L. Ice, 2013: Methods for identifying systematic differential reflectivity biases on the operational WSR-88D Network. Extended Abstract, *36th Conference on Radar Meteorology*, 16–20 September 2013, Breckenridge, CO.

Fiebrich, C. A. and co-authors, 2010: Quality assurance procedures for meso-scale meteorological data. *J. Atmos. Oceanic Technol.*, **27**, 1565–1582.

Giagrande, S. and A. Ryshkov, 2008: Estimation of rainfall based on the results of polarimetric echo classification. *J. Appl. Meteor*., **47**, 2445–2462.

Goodison, B.E. and D. Yang, 1996: In situ measurements of solid precipitation in high latitudes: the need for correction. *Proceedings of the Workshop on the ACSYS Solid Precipitation Climatology Project*, WMO/TD-739, WCRP-93, 3–17.

Groisman, P. Ya., and D. R. Legates, 1994: The accuracy of United States precipitation data. *Bull. Amer. Meteor. Soc.*, **75**, 215–227.

Hoban, N. P., J. G. Cunningham, and W. D. Zittel, 2014: Estimating Systematic WSR-88D differential reflectivity biases using Bragg Scattering. *30th Conf. on Environmental Information Processing Technologies*, Amer. Met. Society, 2–6 February 2014, Atlanta, Georgia.

Kim, D., B. Nelson, and D. J. Seo, 2009: Characteristics of reprocessed Hydrometeorological Automated Data System (HADS) hourly precipitation data. *Wea. Forecasting*, **24**, 1287–1296.

Krajewski, W. F., G. Villarini, and J. A. Smith, 2010: Radar rainfall uncertainties: Where are we after thirty years. *Bull. Amer. Meteor. Soc.*, **91**, 87–94.

Lin, Y., and K. E. Mitchell, 2005: The NCEP stage II/ IV hourly precipitation analyses: Development and applications. Preprints, *19th Conf. on Hydrology,* San Diego, CA, Amer. Meteor. Soc., Paper 1.2. [Available online at http://ams.confex.com/ams/pdfpapers/83847.pdf.]

Martinaitis, S. M., 2008: Effects of multi-sensor radar and rain gauge data on hydrologic modeling in relatively flat terrain. M. S. thesis, Florida State University, 99 pp. [Available online at http://etd.lib.fsu.edu/theses/available/etd-11102008-150745]

Martinaitis, S. M. and co-authors, 2014: An examination of the impacts of frozen precipitation on gauge networks during winter precipitation events. Extended Abstract, *39th Natl. Wea. Assoc. Annual Meeting*, Salt Lake City, UT, P3.53.

Marzen, J. and H. E. Fuelberg, 2005: Developing a high resolution precipitation dataset for Florida hydrologic studies. *19th Conf. on Hydrology*, New Orleans, LA, Amer. Meteor. Soc., 19 HYDRO J9.2.

Rasmussen, R. and co-authors, 2012: How well are we measuring snow? – The NOAA/FAA/ NCAR Winter Precipitation Test Bed. *Bull. Amer. Meteor. Soc*., **93**, 811–829.

Ryzhkov, A. V., M. Diederich, P. Zhang, and C. Simmer, 2014: Potential utilization of specific attenuation for rainfall estimation, mitigation of partial beam blockage, and radar networking. *J. Atmos. Oceanic Technol*., **31**, 599–619.

Sieck, L. C., S. J. Burges, and M. Steiner, 2007: Challenges in obtaining reliable measurements of point rainfall, *Water Resour. Res*., **43**, W01420, doi:10.1029/2005WR004519.

Smith, J. A., D. J. Seo, M. L. Baeck, and M. D. Hudlow, 1996: An intercomparison study of NEXRAD precipitation estimates. *Water Resour. Res.*, **32**, 2035–2046.

Steiner, M., J. A. Smith, S. J. Burges, C. V. Alonso, and R. W. Darden, 1999: Effect of bias adjustment and rain gauge data quality control on radar rainfall estimation. *Water Resour. Res.*, **35**, 2487–2503

Tang, L., J. Zhang, C. Langston, J. Krause, K. Howard, and V. Lakshmanan, 2014: A physically based precipitation/non-precipitation radar echo classifier using polarimetric and environmental data in a real-time national system. *Wea. Forecasting*. doi:10.1175/WAF-D-13-00072.1, in press.

Wang, Y., P. Zhang, A. Ryzhkov, J. Zhang, P. Chang, 2014: Utilization of specific attenuation for tropical rainfall estimation in complex terrain. *J. Hydrometeor.*, doi:10.1175/JHM-D-14-0003.1, in press.

Wilson, J. W. and E. A. Brandes, 1979: Radar measurement of rainfall: A summary. *Bull. Amer. Meteor. Soc.*, **60**, 1048-1058.

Zhang, J., and Y. Qi, 2010: A Real-time Algorithm for the Correction of Bright Band Effects in Radar-Derived QPE. *J. Hydrometeor.,* **11**, 1157–1171.

Zhang, J., and co-authors, 2011: National Mosaic and Multi-Sensor QPE (NMQ) system: Description, results, and future plans. *Bull. Amer. Meteor. Soc.*, **92**, 1321–1338.

Zhang, J. and co-authors, 2014: Initial operating capabilities of quantitative precipitation estimates in the Multi-Radar Multi-System. Extended Abstract, *28th Conf. of Hydrology*, Amer. Met. Society, 2–6 Feb 2014, Atlanta, GA.

APPENDIX:

Summary of cool-season weather events evaluated. Data evaluated was for a 24-hr period ending at 1200 UTC and includes the northwest/southeast corners of the evaluated region.

Date	***NW/SE Box Coordinates***	***Event Summary***
6 December 2013	42ºN, -103ºW 29ºN, -77.7ºW	Thunderstorms and wintry precipitation developed along and behind a strong cold front. Precipitation stretched from TX northeastward into OH.
7 December 2013	44ºN, -100ºW 29ºN, -70.4ºW	Precipitation re-developed along and behind a nearly stationary front. By 1200 UTC on 7 December, sleet/snow blanketed OK northeastward into IL and with 50–250 mm totals and locally higher amounts.
22 December 2013	44ºN, -103ºW 29ºN, -73.4ºW	Strong cold front affected the Plains, Mid-South, and Midwest with rainfall totals of 70–150 mm falling along the front and 100–220 mm of snow behind it. Some areas were impacted severely by freezing rain, especially central/southern MI.
23 December 2013	42ºN, -94ºW 29ºN, -68.7ºW	Thunderstorms and heavy rain developed along a slow moving cold front over the Southeast and Mid-Atlantic states. Rainfall totals ranged from 70–170 mm.
6 January 2014	46ºN, -95ºW 35ºN, -72.0ºW	Moderate to heavy snow developed along and behind a cold front. Snow and rain fell from MO northeastward into New England with snow amounts as high as 350 mm in IN/MI.
29 January 2014	40ºN, -94ºW 28ºN, -71.0ºW	Rain, freezing rain, sleet and some snow associated with developing low pressure fell across the southeast United States. Ice accumulations of 5 to 12.5 mm occurred near the coast.
3 February 2014	45ºN, -102ºW 29ºN, -70.2ºW	Heavy rain and wintry precipitation fell along and behind a cold front that stretched from TX northeastward into the OH valley.
5 February 2014	45ºN, -102ºW 29ºN, -70.2ºW	Heavy rain and wintry precipitation developed along and behind a weak stationary front stretching from the southeast into WV. Rain ranged from 30–80 mm from AR to KY.
13 February 2014	42ºN, -92ºW 29ºN, -66.7ºW	Rain and wintry precipitation developed over the southeast United States and Mid-Atlantic states.
3 March 2014	42ºN, -104ºW 29ºN, -78.7ºW	Rain and wintry precipitation developed along and behind a strong cold front stretching from TX to MD. Rainfall totals of 40–80 mm over AR to KY. Sleet and snow totals of 50–150 mm over portions of OK into MO.
17 March 2014	40ºN, -96ºW 28ºN, -73.0ºW	Heavy rain, sleet and snow developed in response to a mid-latitude cyclone tracking across the South. Rain ranged from 60–150 mm over AL/FL/GA.